Photoluminescence Study of Defects in ZnO Coated Polyacrylonitrile Nanofibers

Daina Damberga, Roman Viter, Viktoriia Fedorenko, Igor Iatsunskyi,
Emerson Coy, Octavio Graniel, Sebastien Balme, Philippe Miele, Mikhael
Bechelany

Photoluminescence Study of Defects in ZnO Coated Polyacrylonitrile Nanofibers

Daina Damberga[1], Roman Viter[1*], Viktoriia Fedorenko[1], Igor Iatsunskyi[2*], Emerson Coy[2], Octavio Graniel[3], Sébastien Balme[3], Philippe Miele[3], Mikhael Bechelany[*3]

[1] Institute of Atomic Physics and Spectroscopy, University of Latvia, Jelgavas 3, Riga, Latvia, LV-1004

[2] NanoBioMedical Centre, Adam Mickiewicz University in Poznan, Wszechnicy Piastowskiej str. 3, 61-614 Poznan, Poland

[3] Institut Européen des Membranes, IEM, UMR 5635, ENSCM, CNRS, Univ Montpellier, Montpellier, France

Corresponding authors: roman.viter@lu.lv, yatsunskiy@gmail.com, mikhael.bechelany@umontpellier.fr

Abstract

Core-shell nanostructures of one-dimensional (1D) polyacrylonitrile (PAN)/zinc oxide (ZnO) were obtained by combining atomic layer deposition (ALD) and electrospinning. Nanofibers with different ZnO thicknesses were synthesized and investigated. The present work offers novel information about 1D ZnO structural defects and activation energies (E_a) by performing photoluminescence (PL) measurements. PL measurements of 1D ZnO/PAN samples were investigated from 77 K to 273 K (room temperature). By analyzing the obtained data of the emission spectrum, E_a and temperature coefficients were calculated. The results let us suggest an approximate model of defects in 1D ZnO/PAN structures. It was observed that optical properties

are strongly related to the structural properties of the obtained 1D materials i.e., the calculation of the concentration of defects in the ZnO layer was done by analyzing the optical measurements. These investigations allow predicting the properties of the materials and opens up a new roadmap for reliable sensing.

Introduction

ZnO is an n-type semiconductor with a direct wide-band gap that has been employed in optical, gas sensing, and biosensing applications [1–9]. Currently, the deposition of ZnO as a thin film can be achieved by sol-gel, magnetron sputtering, chemical vapor deposition (CVD), and atomic layer deposition (ALD) methods [1,10,11]. Among them, ALD allows the synthesis of conformal thin films that can undergo a phase transition from amorphous to crystalline as the layer thickness is increased [12].

Coupled with this phase transition, it has been observed that the underlying substrate of ZnO nanolayers has an impact on its properties (grain size, crystallinity, band gap and photoluminescence) [13,14]. For instance, it was shown that the growth of ZnO on an Al_2O_3 sublayer stimulates the crystallization of ZnO films at lower thicknesses when compared to ZnO ALD layers grown on silicon (Si) substrates [15].

Equally important, electrospinning is a well-established technique that allows the fabrication of one dimensional (1D) nanostructures with a high-degree of porosity and a high surface-to-volume ratio. In particular, the combination of electrospinning and ALD offer the possibility of fabricating materials with advanced structural and optical properties [16]. Recently, it was shown that ZnO nanolayers and ZnO/Al_2O_3 nanolaminates could be successfully deposited on electrospun polyacrylonitrile (PAN) nanofibers [17,18]. The obtained samples showed a high

photoluminescence emission (10000:1 gain) compared to samples deposited on glass and Si substrates.

It is well-known that ZnO has two emission bands: an ultraviolet (UV) band (360-390 nm) related to excitons and a visible band (405-700 nm) related to structural defects [19,20]. Moreover, it has been shown that the UV emission of ZnO can be diminished by the nanolayer thickness when the ZnO thickness is compared with the size of the exciton Bohr radius of ZnO (~ 2.3 nm) [18]. In a similar way, the visible emission of ZnO is based on defect levels such as zinc vacancies (3.03-3.15 eV)[12,20], zinc interstitials (3.1-3.22 eV), oxygen vacancy (2.76-2.95 eV), and oxygen interstitials (2.12-2.25 eV) that are present in the material[12,21,22]. Correspondingly, by analyzing the correlation between photoluminescence (PL) and structural properties it is possible to estimate the defect concentrations in ZnO nanostructures [23]. The calculated concentrations of defect levels and quantum efficiency of the photoluminescence were evaluated by measuring PL intensity vs excitation power at low temperatures [23]. The temperature quenching of ZnO photoluminescence can provide activation energies for defect levels[24] and binding energies for excitons [25]. Therefore, investigation of PL spectra at different excitation powers and PL temperature quenching can provide information about defects and role of the structural parameters (depletion layer, defect concentration, thicknesses, etc.) to optical properties of ZnO nanostructures[23,24]

Returning to ALD, it has been observed that nanostructures deposited by this technique display an amorphous-to-crystalline transition [26]. Besides, the deposition of ZnO and Al_2O_3/ZnO layers on PAN template stimulates the formation of a crystalline structure [17]. Interestingly, the transition from amorphous to crystalline phase of ZnO was observed at ZnO thicknesses of 20 nm and 5 nm for ZnO and Al_2O_3/ZnO layers on PAN, respectively [17,18]. This transition was much

lower when compared to ZnO films deposited by ALD on Si (~ 50 nm) [12,16]. Bearing this in mind, both crystallization and defect healing of ZnO depend on the film thickness, and lead to changes in the structural and optical properties of the ZnO film [12]. Similarly, it has been suggested that strain effects on the PAN surface could stimulate growth and enhancement of the optical properties of ZnO deposited by ALD. Despite some reports suggesting that the growth of the ZnO sublayer thickness increases the work function and quenches PL intensity in ZnO/Al_2O_3 nanolaminates[15,18] deposited by ALD on PAN nanofibers, no correlation between the film growth, strain effects, and quantum confinement effects with the optical and structural properties of ZnO layers deposited by ALD on PAN nanofibers has been reported so far.

In the present paper high-surface-area core-shell 1D ZnO/PAN structures were prepared by a combination of electrospinning[27] and ALD techniques [28,29]. The morphology, crystallinity, and optical properties of these core-shell structures have been investigated by transmission electron microscopy (TEM), scanning electron microscopy (SEM), X-ray diffraction (XRD), and PL methods. The activation energies and exciton binding energies were obtained from the ZnO PL temperature quenching. The defect concentrations were calculated from the excitation power dependence of the ZnO PL measured at low temperatures. Firstly for ZnO ALD layers, an analysis of the structural and optical properties of ZnO layers deposited by ALD with different thicknesses deposited on PAN nanofibers were performed. The ZnO PL intensity and peak position was analyzed by taking into account the defect concentration, thickness/surface-to-volume ratio, strain effects, and crystallinity. Finally, the mechanisms of correlation between the optical and structural properties in ZnO ALD layers of different thicknesses are presented.

Experimental Section

Materials

Polyacrylonitrile (PAN, Mwt 150 000, CAS No. 25014-41-9),N,N-dimethylformamide (DMF, 98%, CAS No. 68-12-2), and diethylzinc ((DEZ), Zn $(CH_2CH_3)_2$, 95%, CAS No. 557-20-0) were purchased from Sigma-Aldrich.

Synthesis of PAN nanofibers

First, PAN (10 g) was dissolved in DMF (100 ml) for a final concentration of 10 wt % PAN. The PAN/DMF solution was stirred for one hour and then it was heated in an oil bath at 80 °C for 10 min. The electrospinning was carried out at room temperature (20°C) in air with an applied voltage of 17 kV and a pump rate of 0.2 ml per hour. The home-made electrospinning machine consisted of a syringe pump (KDS 100) with a needle diameter of 0.7 mm and a generator (HPx 600 605, Physical Instruments). The syringe needle was connected to the positive entry of the voltage generator while the negative entry was connected to the collector at a distance of 25 cm from the syringe needle spike. When the stretched solution landed on the collector, a long fiber with an approximate diameter of 250 to 350 nm was produced [16].

Atomic layer deposition of ZnO

ZnO was deposited at 100 °C using sequential exposures of DEZ and deionized (DI) water separated by a purge of dry argon (flow rate of 100 sccm). The deposition cycle is described as follows: (a) 2 s pulse of DEZ, 30 s exposure, and 50 s purge with argon; (b) 3 s pulse of H_2O, 40

s of exposure, and 60 s purge with argon. The growth rate was typically 2 Å/cycle for ZnO [16,26,30].

Structural characterization of 1D ZnO nanostructures

Scanning electron microscopy (SEM) was used to analyze the morphology of the nanofibers using a JEOL JSM 7001F microscope. X-ray diffraction (XRD) was obtained with a PANAlytical Xpert-PRO diffractometer equipped with an accelerator detector using Ni-filtered Cu-radiation with a wavelength of 1.54 A. Transmission Electron Microscopy (TEM) images were obtained with a JEOL ARM 200F high resolution transmission electron microscope (200 kV) coupled with an JED2300 EDX analyzer.

Optical characterization of 1D ZnO nanostructures

A nitrogen laser with a $\lambda=337$ nm, a pulse duration of 10 ns, a power of 2.88 mW, and a spot size of 3 mm was used as the excitation source. PL was measured by an Ocean Optics HR2000+ spectrometer. The emitted light was collected using a collimating lens assembled with an optical fiber. PL spectra were collected in the range of 360 nm - 900 nm. The integration time varied from 1 s to 4 s depending on the PL intensity.

The PL power dependence measurements were performed by using four neutral density filters to achieve different excitation powers. The laser power was varied between 0.20 mW and 2.88 mW. The PL measurements were obtained at 77 K. In addition, PL temperature-dependent measurements were performed in a temperature range of 77 K to 273 K. The temperature was controlled by a Type-K thermocouple and measured with a step of -5±1 K. The error bars were calculated as average from 3 measurements.

Results

Structural properties of 1D ZnO/PAN

Figure 1a shows the SEM image of one-dimensional (1D) polyacrylonitrile (PAN)/zinc oxide (ZnO) obtained with 300 s electrospinning time and coated with 50 cycles of ZnO by ALD. The obtained SEM images confirm the conformal ZnO coating over the PAN nanofibers. The average diameter of the nanofibers is about 500 ± 100 nm. The surface of the ZnO nanofibers is relatively granular, which may indicate the polycrystalline structure of the deposited thin film. XRD spectra of the 1D ZnO nanostructures display characteristic ZnO peaks for the 20 nm, 15 nm, and 10 nm ZnO thicknesses (Table 1.). The most intense peaks can be assigned to the hexagonal würtzite planes of (100), (002), and (101) of ZnO. In Figure 1b, a peak shift towards higher values and a decrease of the peak width for higher ZnO layer thicknesses was observed. This is in agreement with previous results [31] where it was demonstrated that, as the thickness of the ZnO increases, more strain is put on the organic core that results in an improvement of the crystallinity. The broadening of the peaks can be explained by a decrease of the grain size and strain effects[22]. The absence of the peaks for the 5 nm and 2.5 nm ZnO thicknesses could be related to the low crystallite size and/or the amorphous nature of the ZnO.
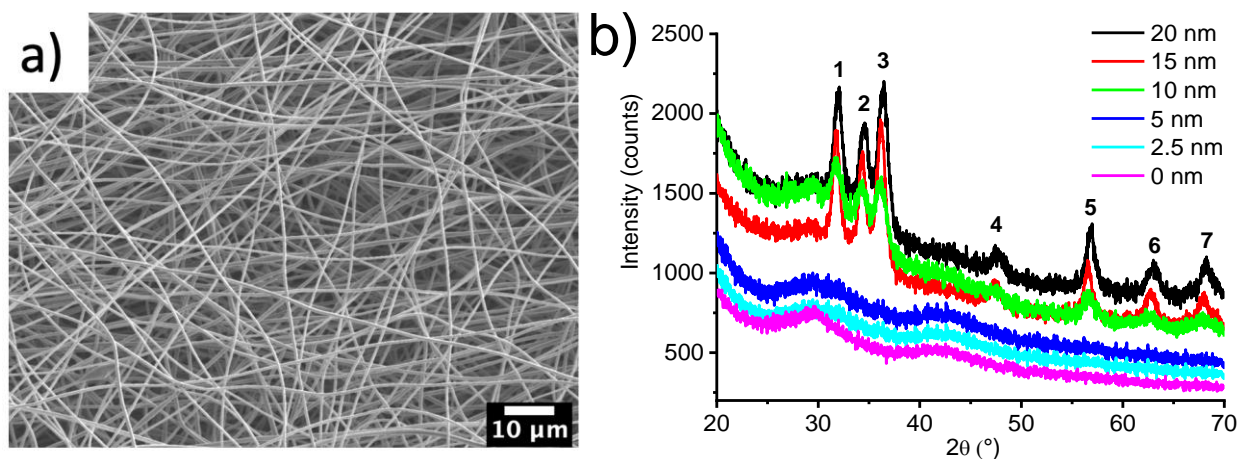
Figure 1. (a) SEM images of the 1D ZnO nanostructures obtained with 300 s electrospinning time and coated with 50 cycles of ZnO by ALD at 373 K. (b) XRD data for samples of ZnO with thicknesses of 0, 2.5, 5, 10, 15, 20 nm.

Table 1. XRD peak positions for 1D ZnO nanostructures with varying thicknesses

Thickness (nm)	Peak position (°)						
	1	2	3	4	5	6	7
20	32.25	34.83	36.68	47.73	56.84	62.91	68.19
15	32.08	34.67	36.53	47.48	56.58	62.78	67.94
10	31.89	34.49	36.34	-	56.62	62.66	67.87
Reference[7,16]	31.74	34.42	36.22	47.53	56.61	62.6	68.03

The crystallinity of the ZnO films was investigated by TEM. The TEM measurements (Figure 2) demonstrate the crystalline nature of the samples with a ZnO film thickness of 5 nm [16]. Furthermore, it can be observed that the ZnO films have a granular structure. The average grain

size was calculated using an elliptical shape fitting (Figure 2d). By analyzing the gran size values

we observed that as the thickness of the ZnO films decreases the grain size also decreases.
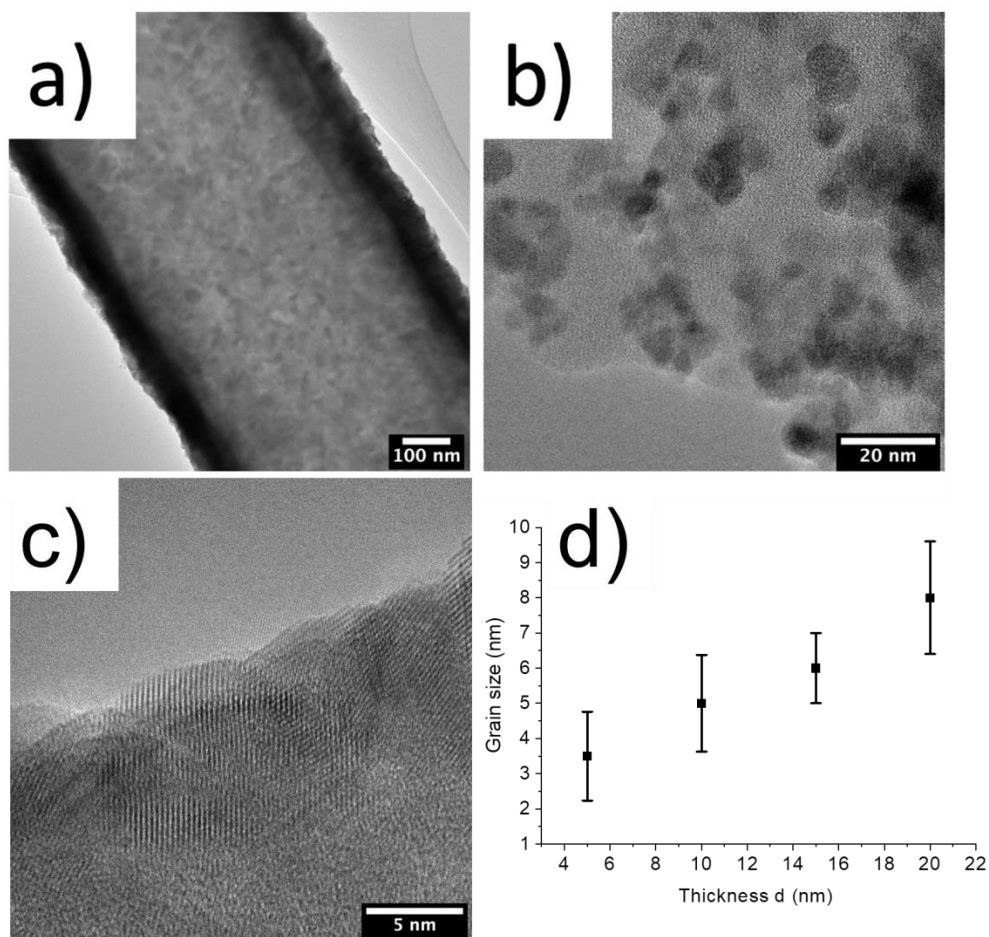
Figure 2. TEM images of a) 1D ZnO deposited on PAN nanofibers with 5 nm thickness and b, c)

the crystallites of ZnO on the PAN surface, d) TEM data of ZnO grain size dependence on ZnO

layer thickness

ZnO layer thickness influence on PL spectra

The optical properties of 1D ZnO/PAN nanostructures with ZnO thickness 20, 15, 10, 5 and 2.5

nm were investigated by PL measurements (Figure 3a); The samples with 20 nm and 15 nm of

ZnO have strong emission bands in the UV and visible range that can be related to free excitonic

and surface defects, respectively [3,24]. We also observed that, as the ZnO film thickness decreases, the UV and visible emissions intensity decreases. Similarly, the ratio of the UV/VIS emissions significantly decreases with the decrease of the ZnO film thickness (Figure 3b). It is widely known that the PL of ZnO significantly depends on the crystallinity of the sample [12,15]. The comparative analysis between XRD and PL of the core-shell structures with different ZnO thin film thicknesses display a correlation between the XRD peak intensity and the ratio of the UV/VIS emissions. These results confirm the crystallinity of the samples covered with a 5 nm ZnO film. However, the samples with a 2.5 nm ZnO film were not possible to investigate due to the XRD detection limit of 4.5 nm.
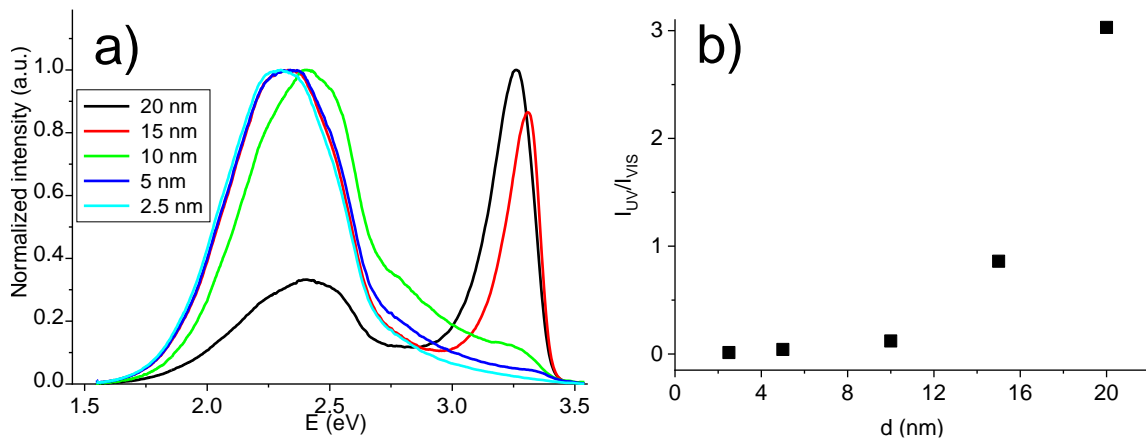
Figure 3. a) PL spectra: Normalized peak positions at 77 K for different 1D ZnO thicknesses excited by nitrogen laser E=3.68 eV. b) UV/VIS emission ratio for 1D ZnO/PAN samples with different ZnO thicknesses

By carefully analyzing the PL spectra from Figure 3a, a red shift of the visible emission and a blue shift of the UV emission can be observed as the ZnO film thickness decreases. The red shift of the visible emission is related to band bending [3]. Based on literature,[3] the depletion layer width

increases and is accompanied by a transition of the neutral defects to an ionized state at low temperatures of 77 K. Similarly, the blue shift of the UV band can be related to a quantum confinement effect due to a decrease of the grain size with a decrease of the layer thickness [12,15].

PL dependence on excitation power for 1D ZnO nanofibers

The PL spectra from Figure 4a were deconvoluted with a Gaussian function in *Origin Pro 7* and are shown in Figure 4b. The emission intensity depends on the excitation power (P) as

$$I \sim P^k$$

where the power coefficient (k) is calculated (Table 2.). For bound excitons and defect-level transitions, the parameter k has values lower than one. On the other hand, for free excitons, the value of k is always higher than 1. Therefore, by means of power dependence, we can analyze the type of transitions from the 1D ZnO nanostructures.

Table 2. Peak positions of deconvoluted PL spectra for different ZnO thicknesses and

corresponding power coefficients

Thickness (nm)								
	20	Peak position (eV)	3.31	3.24	3.14	2.89	2.5	2.35
		k	1.01	0.84	0.71	0.97	0.48	0.79
	15	Peak position (eV)	3.33	3.27	3.16	2.87	2.49	2.30
		k	1.03	0.91	0.85	0.81	0.61	0.81
	10	Peak position (eV)		3.22	2.95	2.80	2.53	2.37
		k		0.81	0.86	0.85	0.92	0.78
	5	Peak position		3.20	2.93	2.79	2.52	2.30

		(eV)				
		k	0.98	0.65	0.68	0.74	0.82
	2.5	Peak position (eV)		3.03	2.83	2.50	2.29
		k		0.87	0.89	0.79	0.83

It is worth mentioning that the obtained peak positions for free exciton emission were red shifted 0.015 eV - 0.025 eV when compared to other works in the literature [32]. A possible explanation can be related to strain effects that result in a red shift of the UV emission [32,33]. In addition, ZnO is a well-known piezoelectric material. According to Reshchikov et al.[34], strain effects can result in a variation of the valence and conduction band positions of ZnO, which reduces the band gap and exciton energies.

PL intensity of defect emission depends on parameters of emission centers, such as concentration and cross-capturing coefficients of electrons and holes[35]. The mentioned parameters can be calculated from the dependence of the PL intensity vs. excitation power (Figure 4c).

The PL peak intensity (I) can be calculated as[35]:

$$I = \frac{G}{\frac{G \cdot t_r}{N_d} + \frac{1}{\eta}} \tag{1}$$

Reshchikov et al.[35] made an estimation to the real measurements of the peak intensity (I) and the average laser excitation power (P) taking into account the band-band absorption coefficient (α):

$$I = \int_{x0}^{L} \frac{\alpha \cdot P \cdot e^{-\alpha x}}{\left(\alpha \frac{\tau_r \cdot P \cdot e^{-\alpha x}}{N_d}\right) + \left(\frac{1}{\eta}\right)} dx = \frac{N_d}{\alpha \cdot \tau_r} ln(1 + \frac{N_d \cdot \eta}{\alpha \cdot \tau_r} \cdot P), \tag{2}$$

where η is the quantum efficiency.

Defect levels have a power coefficient lower than 1. This assumption is based on the limitation of the defect concentration in ZnO. Using equation (1), we have estimated the parameters N_d, η and C_p, $t_r= 5$ µs [22] (Figure 4d-f).
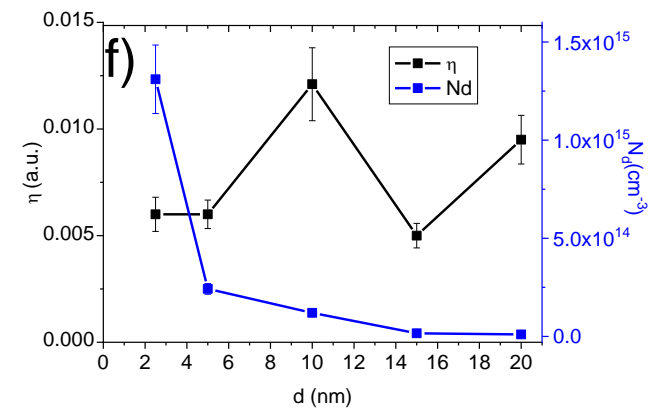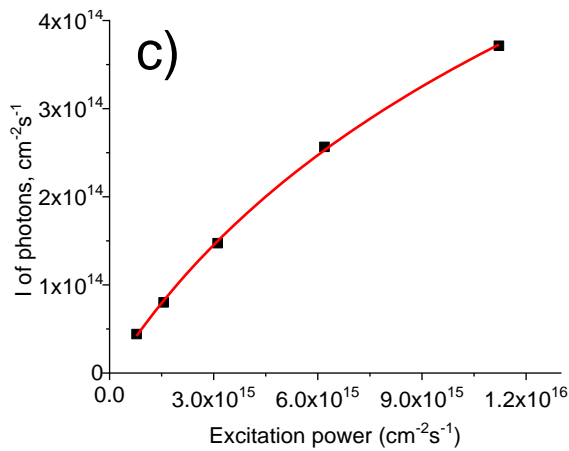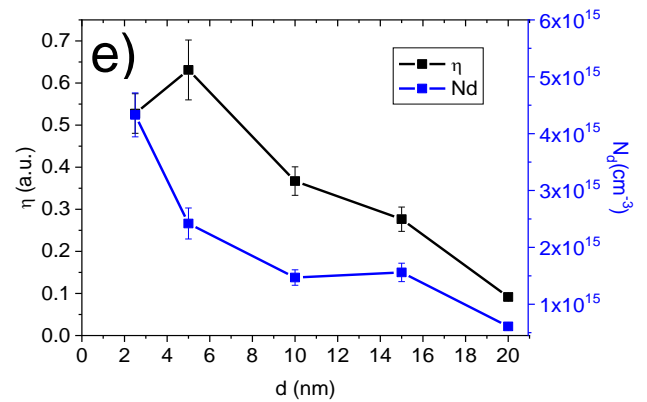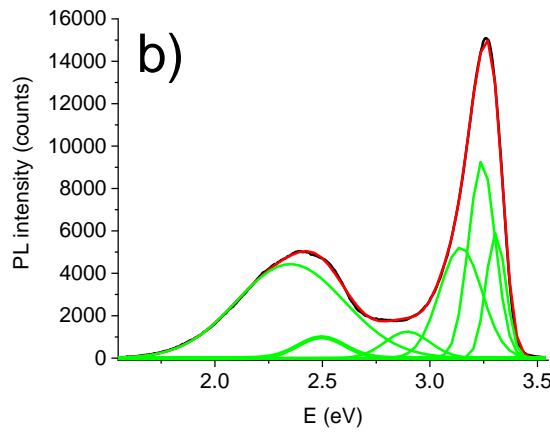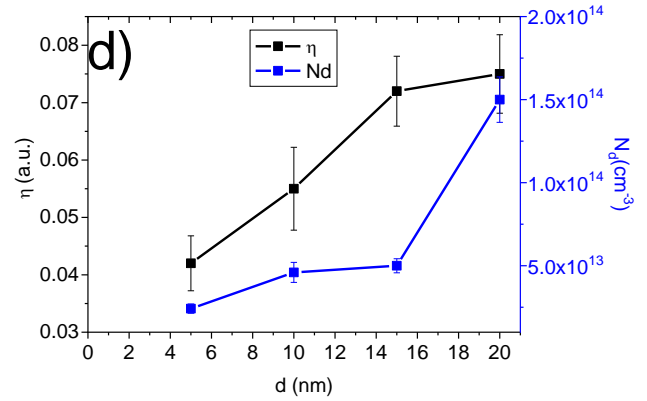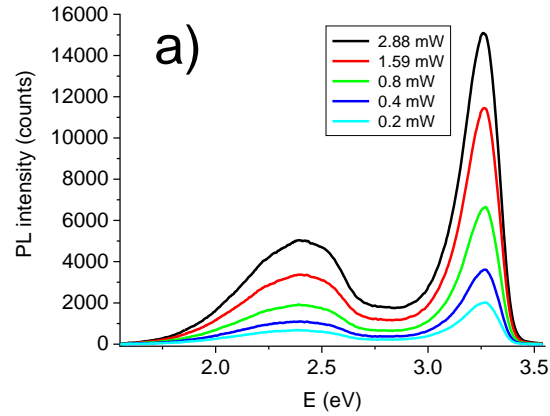
Figure 4. PL power dependence measurements with different neutral density filters for 20 nm sample. Power dependence (a); PL deconvolution with Gaussian function in *Origin Pro 7* at 77 K by using six peaks (b); logarithmic fitting, second peak (c); neutral oxygen vacancy (2.78 – 2.85 eV) (d); singly ionized oxygen vacancy (2.45 – 2.53 eV) (e); doubly ionized oxygen vacancy (2.30 – 2.35 eV) (f)

According to Janotti *et al.*[20] , ZnO has emission peaks centered at the following positions (Figure 5): 3.3-3.4 eV – free exciton emission, 3.24-3.27 eV donor bound excitons/or defect, 3.1-3.22 – Zn interstitials, 3.03 eV – zinc vacancies, 2.76-2.95 eV – ionized Zn interstitials/oxygen vacancies, 2.45-2.6 eV – singly ionized O vacancy, 2.29-2.37 eV – doubly ionized O vacancies. Thus, based on the values shown in Table 2, we can conclude that the decrease of the ZnO thickness results in a quenching of the free exciton emission due to a low crystallinity and a surface band bending. Due to a lower crystallinity, the defect concentration in samples with ZnO thicknesses lower than 15 nm was drastically increased (Figure 3b).
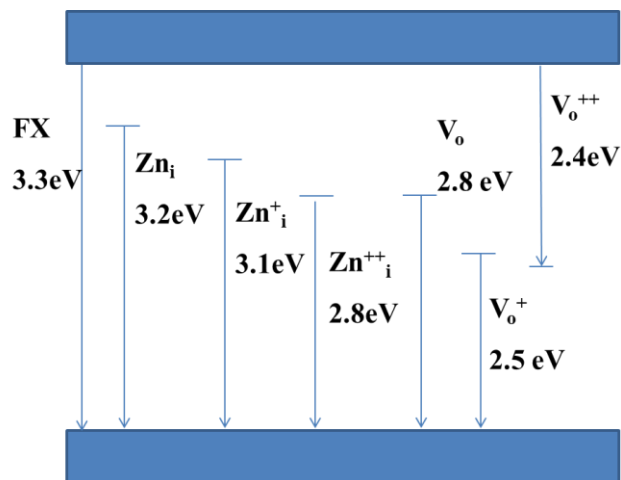
Figure 5. Possible optical transitions and their energies in ZnO nanostructures where FX – free excitons, Zn_i – zinc interstitials, Zn^+_i – ionized zinc interstitials, V_o – oxygen vacancies, V^+_o – ionized oxygen vacancies

The decrease of the ZnO film thickness results in a decrease of the concentration of singly ionized vacancies (peak at 2.5 eV). Similarly, the concentration of doubly ionized vacancies increased with the decrease of the ZnO film thickness (2.3 eV). The observed transitions between neutral and charged vacancies point towards an influence of the band bending, as previously discussed.

Moreover, the quantum efficiency η depends on the concentration of the emission centers. The decrease of the η with the thickness is related to the structural properties of the samples. As it was discussed previously, the ZnO growth improves the crystalline nature of the samples and decreases the surface band bending. This effect results in a decrease of the doubly ionized oxygen vacancy concentration.

Photoluminescence investigations of ZnO defect energies have been performed before [12]. However, numerical values of defect concentration had not been previously obtained by this method. Nonetheless, neutral oxygen vacancy concentration determined by cathodoluminescence for non-stoichiometric ZnO displayed a concentration almost three orders of magnitude higher $(10^{15}\text{-}10^{18}$ cm$^{-3})$ [2] than the result presented in this work $(2.4 \cdot 10^{13}\text{-}1.5 \cdot 10^{15})$ cm^{-3}. On the other hand, the singly ionized oxygen vacancy concentration $(6.1 \cdot 10^{14}\text{-}4.3 \cdot 10^{15})$ cm^{-3} was lower than the one evaluated by EPR $(2 \cdot 10^{14}\,$cm$^{-3})$ in a bulk material [36]. The concentration of doubly ionized oxygen vacancies showed a significant decrease with the growth of the ZnO layer thickness.

PL dependence on temperature for 1D ZnO nanofibers

Temperature-dependent PL measurements provide valuable information on the quenching of the emission. The PL spectra of 1D ZnO nanorods were measured in a temperature range of 77 K-273 K as shown in Figure 6a. The analysis of the peak position, full width at half maximum (FWHM), and intensity showed that, for the peaks in the range of 2.8 eV - 3.33 eV, a red shift of the peak position and a peak FWHM widening occurred. Similarly, for the peaks in the 2.29 eV - 2.6 eV range, a blue shift of the peak position was observed. The effect of the peak shift has been reported previously [25,34]. The increase of the temperature increases the lattice vibrations. Similarly, the increase of both the FWHM and the shift of the peak position are related to electron-phonon interactions. Furthermore, the red and blue shifts are related to emission and absorption of photons.

The quenching of the PL intensity (I) can be described by the following equation [25]:

$$I \sim \frac{1}{1 + A \cdot exp^{-(\frac{E_a}{k_B T})}} \qquad (3)$$

where k_B, A, and T are the Boltzmann constant, proportional coefficient, and absolute temperature, respectively.

The obtained dependences I(T) were plotted in as 1/I vs 1/T and fitted by an exponential function (Figure 6b) to calculate activation energies. We can observe that the values of E_a for the 1D ZnO 20 nm samples is in good correlation to an exciton binding energy of 0.06 eV[37]. The E_a parameter for 1D ZnO with 15 nm thickness was found to be 0.041 eV, which is lower than previous reports [38]. The decrease of the exciton binding energy could be related to the electric field formed near the surface due to surface band bending. Also, the E_a of the visible emission

correlates with values reported in the literature [19,39]. For defect levels, the calculated E_a does not correspond to ionization energies of the defect level as the distance between the defect level and conduction band is more than 0.2 eV - 0.3 eV[20]. The obtained values correspond to energetic distances between radiative and non-radiative transitions (Figure 7). The obtained energies correlate with similar values detected for ZnO samples [19,39].
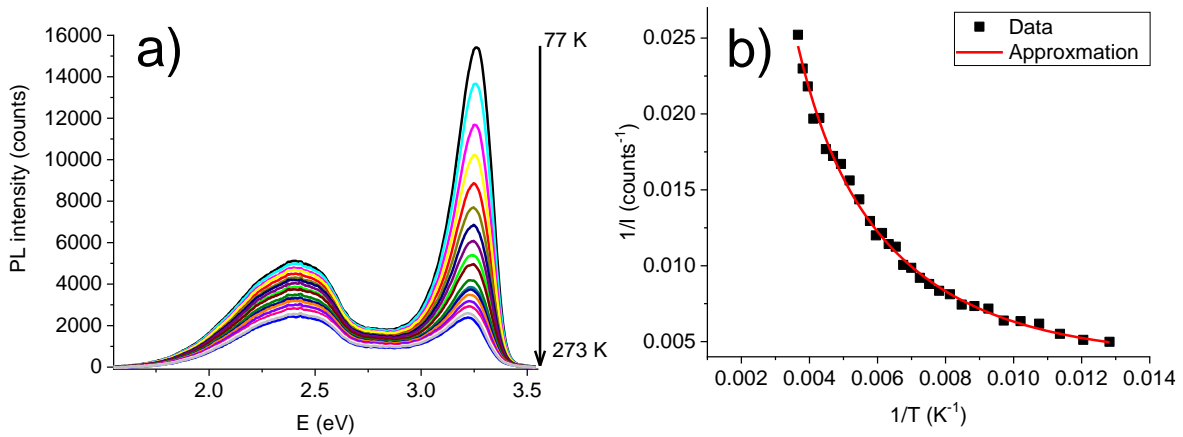

Figure 6. PL temperature dependence for the 20 nm sample (a); exponential approximation for E_a calculations - 20 nm sample and peak 2 is used in the graph (spectra deconvolution shown in Figure 5b)
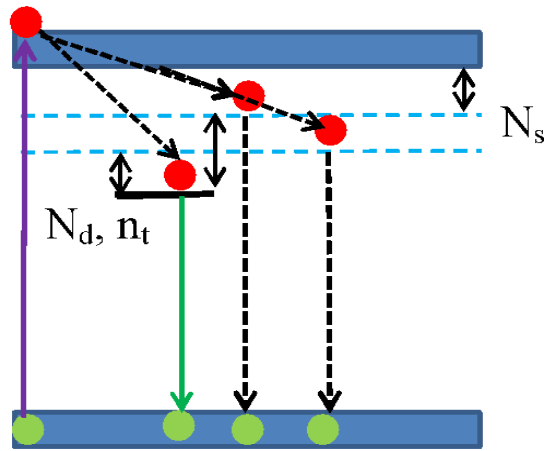
Figure 7. Possible radiative and non-radiative transitions

Quantum efficiency might be proportional to defect concentration for oxygen vacancies V_O and doubly ionized oxygen vacancies V_{O++}. The ratio V_O/ V_{O++} depends on deposited film thickness. The process of oxygen vacancy ionization could cause energy shifts.

Therefore, properties of ZnO/PAN nanostructures can be affected by the depletion layer width (Figure 8). At the beginning stage of the ZnO ALD growth thin layers with low crystallites are formed. The depletion layer is spread within the whole ZnO coating. The increase of the thickness improves the ALD ZnO crystallinity and reduces the depletion layer width. ZnO films deposited by ALD with a thickness of 15 nm are interstates in between partially depleted and fully depleted layer. The tailoring of depletion layer in ALD ZnO/PAN nanofibers could be useful for optical applications, particularly for gas and chemical sensors.
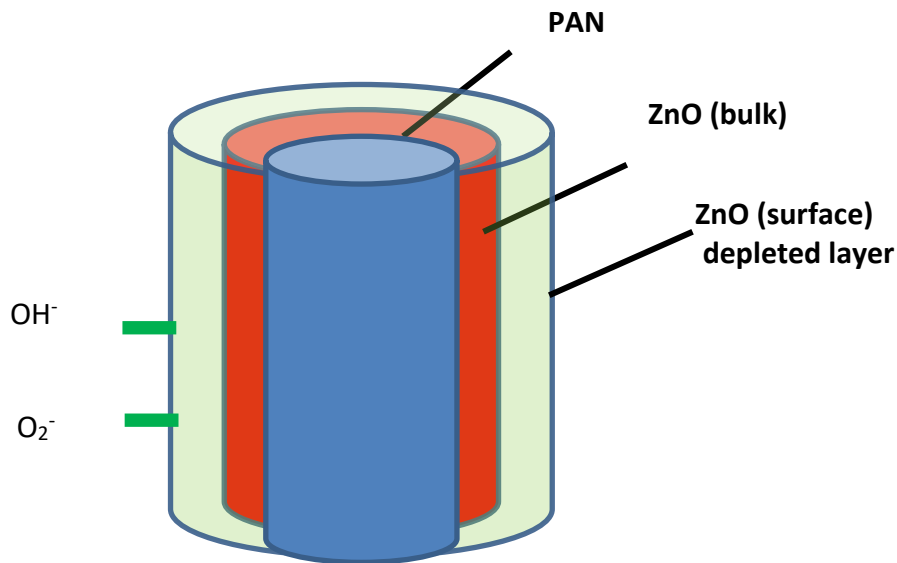
Figure 8. Thin films with electrospun PAN nanofibers as core and ZnO layer as shell layer.

Conclusions

Core-shell PAN/ZnO nanofibers were prepared by combining ALD and electrospinning. The increase of the ZnO thickness results in an improvement of the crystallinity, a decrease of the defect concentration, and an increase of the strain. An amorphous to crystalline phase transition occurs for ZnO film thicknesses higher than 10 nm. Due to the strain effects, shifts of the XRD and PL peaks were observed. A careful analysis of defect states in ZnO showed that the samples have two common peaks that correspond to singly ionized and doubly ionized oxygen vacancies. These defects are responsible for changes in the visible portion of the PL emission. In addition, defect passivation takes places during ZnO growth. Quantum efficiency correlates with defect concentration. Adsorbed surface species (O^{2-}, OH^-) influence binding energy of free excitons. PL UV peak shift of exciton emission from 20 nm – 15 nm ZnO is explained by the decrease of

grain size. Excitonic peaks for ZnO 15 nm and 20 nm are shifted towards lower energies

compared to literature data[38] because of the surface strain. The quenching of UV emission in

samples lower than ZnO 15 nm results from lower crystallinity, higher defect concentrations and

surface band bending. The methodology proposed in the present work allows analyzing

correlation between structural and optical properties of 1D ZnO nanostructures.

Acknowledgements

References

(1)   Shakti, N.; Gupta, P. S. Structural and Optical Properties of Sol-Gel Prepared ZnO Thin
         Film. *Appl. Phys. Res.* **2010**, *2* (1), 19. https://doi.org/10.5539/apr.v2n1p19.
(2)   Ton-That, C.; Weston, L.; Phillips, M. R. Characteristics of Point Defects in the Green
         Luminescence from Zn- and O-Rich ZnO. *Phys. Rev. B - Condens. Matter Mater. Phys.*
         2012, *86* (11), 115205. https://doi.org/10.1103/PhysRevB.86.115205.
(3)   Liao, Z. M.; Zhang, H. Z.; Zhou, Y. B.; Xu, J.; Zhang, J. M.; Yu, D. P. Surface Effects on
         Photoluminescence of Single ZnO Nanowires. *Phys. Lett. Sect. A Gen. At. Solid State
         Phys.* **2008**, *372* (24), 4505–4509. https://doi.org/10.1016/j.physleta.2008.04.013.
(4)   Ning, Y.; Zhang, Z.; Teng, F.; Fang, X. Novel Transparent and Self-Powered UV
         Photodetector Based on Crossed ZnO Nanofiber Array Homojunction. *Small* **2018**, *14*
         (13), 1703754. https://doi.org/10.1002/smll.201703754.
(5)   Liang, Y. C.; Zhao, Q.; Liu, K. K.; Liu, Q.; Lu, X. L.; Wu, X. Y.; Lu, Y. J.; Dong, L.;
         Shan, C. X. Ultrasensitive Mechano-Stimuli Luminescence Enhancement in ZnO
         Nanoparticles. *J. Phys. Chem. Lett.* **2019**, *10* (13), 3557–3562.
         https://doi.org/10.1021/acs.jpclett.9b01092.
(6)   Hu, K.; Teng, F.; Zheng, L.; Yu, P.; Zhang, Z.; Chen, H.; Fang, X. Binary Response
         Se/ZnO p-n Heterojunction UV Photodetector with High on/off Ratio and Fast Speed.
         Laser Photonics Rev. **2017**, *11* (1), 1600257. https://doi.org/10.1002/lpor.201600257.
(7)   Fang, X.; Bando, Y.; Gautam, U. K.; Zhai, T.; Zeng, H.; Xu, X.; Liao, M.; Golberg, D.
         ZnO and ZnS Nanostructures: Ultraviolet-Light Emitters, Lasers, and Sensors; *Critical
         Reviews in Solid State and Materials Sciences* **2009**, *34* (3-4), 190-223.
         https://doi.org/10.1080/10408430903245393.
(8)   Baitimirova, M.; Andzane, J.; Viter, R.; Fraisse, B.; Graniel, O.; Bechelany, M.; Watt, J.;

Peckus, D.; Tamulevicius, S.; Erts, D. Improved Crystalline Structure and Enhanced Photoluminescence of ZnO Nanolayers in Bi2Se3/ZnO Heterostructures. *J. Phys. Chem. C* **2019**, *123* (51), 31156–31166. https://doi.org/10.1021/acs.jpcc.9b08417.

(9)   Zhao, B.; Wang, F.; Chen, H.; Zheng, L.; Su, L.; Zhao, D.; Fang, X. An Ultrahigh Responsivity (9.7 MA W−1) Self-Powered Solar-Blind Photodetector Based on Individual ZnO–Ga2O3 Heterostructures. *Adv. Funct. Mater.* **2017**, *27* (17), 1–8. https://doi.org/10.1002/adfm.201700264.

(10)   Cao, Y.; Galoppini, E.; Reyes, P. I.; Duan, Z.; Lu, Y. Morphology Effects on the Biofunctionalization of Nanostructured ZnO. *Langmuir* **2012**, *28* (21), 7947–7951. https://doi.org/10.1021/la3006037.

(11)   Graniel, O.; Fedorenko, V.; Viter, R.; Iatsunskyi, I.; Nowaczyk, G.; Weber, M.; Załęski, K.; Jurga, S.; Smyntyna, V.; Miele, P.; et al. Optical Properties of ZnO Deposited by Atomic Layer Deposition (ALD) on Si Nanowires. *Mater. Sci. Eng. B Solid-State Mater. Adv. Technol.* **2018**, *236–237* (October 2017), 139–146. https://doi.org/10.1016/j.mseb.2018.11.007.

(12)   Chaaya, A. A.; Viter, R.; Bechelany, M.; Alute, Z.; Erts, D.; Zalesskaya, A.; Kovalevskis, K.; Rouessac, V.; Smyntyna, V.; Miele, P. Evolution of Microstructure and Related Optical Properties of ZnO Grown by Atomic Layer Deposition. *Beilstein J. Nanotechnol.* **2013**, *4* (1), 690–698. https://doi.org/10.3762/bjnano.4.78.

(13)   Singh, A.; Mathur, A.; Pal, D.; Sengupta, A.; Singh, R.; Chattopadhyay, S. Near Room Temperature Atomic Layer Deposition of ZnO Thin Films on Poly (Methyl Methacrylate) (PMMA) Templates: A Study of Structure, Morphology and Photoluminescence of ZnO as an Effect of Template Confinement. *Vacuum* **2019**, *161* (October 2018), 398–403. https://doi.org/10.1016/j.vacuum.2019.01.006.

(14)   Miikkulainen, V.; Leskelä, M.; Ritala, M.; Puurunen, R. L. Crystallinity of Inorganic Films Grown by Atomic Layer Deposition: Overview and General Trends. *J. Appl. Phys.* **2013**, *113* (2), 2. https://doi.org/10.1063/1.4757907.

(15)   Chaaya, A. A.; Viter, R.; Baleviciute, I.; Bechelany, M.; Ramanavicius, A.; Gertnere, Z.; Erts, D.; Smyntyna, V.; Miele, P. Tuning Optical Properties of Al2O3/ZnO Nanolaminates Synthesized by Atomic Layer Deposition. *J. Phys. Chem. C* **2014**, *118* (7), 3811–3819. https://doi.org/10.1021/jp411970w.

(16)   Viter, R.; Abou Chaaya, A.; Iatsunskyi, I.; Nowaczyk, G.; Kovalevskis, K.; Erts, D.; Miele, P.; Smyntyna, V.; Bechelany, M. Tuning of ZnO 1D Nanostructures by Atomic Layer Deposition and Electrospinning for Optical Gas Sensor Applications. *Nanotechnology* **2015**, *26* (10), 105501. https://doi.org/10.1088/0957-4484/26/10/105501.

(17)   Viter, R.; Iatsunskyi, I.; Fedorenko, V.; Tumenas, S.; Balevicius, Z.; Ramanavicius, A.; Balme, S.; Kempiński, M.; Nowaczyk, G.; Jurga, S.; et al. Enhancement of Electronic and Optical Properties of ZnO/Al 2 O 3 Nanolaminate Coated Electrospun Nanofibers. *J. Phys. Chem. C* **2016**, *120* (9), 5124–5132. https://doi.org/10.1021/acs.jpcc.5b12263.

(18)   Iatsunskyi, I.; Vasylenko, A.; Viter, R.; Kempiński, M.; Nowaczyk, G.; Jurga, S.; Bechelany, M. Tailoring of the Electronic Properties of ZnO-Polyacrylonitrile Nanofibers: Experiment and Theory. *Appl. Surf. Sci.* **2017**, *411*, 494–501. https://doi.org/10.1016/j.apsusc.2017.03.111.

(19)   Bethke, S.; Pan, H.; Wessels, B. W. Luminescence of Heteroepitaxial Zinc Oxide. *Appl. Phys. Lett.* **1988**, *52* (2), 138–140. https://doi.org/10.1063/1.99030.

(20)   Janotti, A.; Van De Walle, C. G. Native Point Defects in ZnO. *Phys. Rev. B - Condens. Matter Mater. Phys.* **2007**, *76* (16), 165202. https://doi.org/10.1103/PhysRevB.76.165202.

(21)   Sheetz, R. M.; Ponomareva, I.; Richter, E.; Andriotis, A. N.; Menon, M. Defect-Induced Optical Absorption in the Visible Range in ZnO Nanowires. *Phys. Rev. B - Condens. Matter Mater. Phys.* **2009**, *80* (19), 195314. https://doi.org/10.1103/PhysRevB.80.195314.

(22)   Li, M.; Xing, G.; Xing, G.; Wu, B.; Wu, T.; Zhang, X.; Sum, T. C. Origin of Green Emission and Charge Trapping Dynamics in ZnO Nanowires. *Phys. Rev. B - Condens. Matter Mater. Phys.* **2013**, *87* (11), 115309. https://doi.org/10.1103/PhysRevB.87.115309.

(23)   Reshchikov, M. A.; Usikov, A.; Helava, H.; Makarov, Y.; Prozheeva, V.; Makkonen, I.; Tuomisto, F.; Leach, J. H.; Udwary, K. Evaluation of the Concentration of Point Defects in GaN. *Sci. Rep.* **2017**, *7* (1), 1–11. https://doi.org/10.1038/s41598-017-08570-1.

(24)   Foreman, J. V.; Simmons, J. G.; Baughman, W. E.; Liu, J.; Everitt, H. O. Localized Excitons Mediate Defect Emission in ZnO Powders. *J. Appl. Phys.* **2013**, *113* (13), 133513. https://doi.org/10.1063/1.4798359.

(25)   Reshchikov, M. A.; Morkǫ, H. Luminescence Properties of Defects in GaN. *J. Appl. Phys.* **2005**, *97* (6), 5–19. https://doi.org/10.1063/1.1868059.

(26)   Raghavan, R.; Bechelany, M.; Parlinska, M.; Frey, D.; Mook, W. M.; Beyer, A.; Michler, J.; Utke, I. Nanocrystalline-to-Amorphous Transition in Nanolaminates Grown by Low Temperature Atomic Layer Deposition and Related Mechanical Properties. *Appl. Phys. Lett.* **2012**, *100* (19), 191912. https://doi.org/10.1063/1.4711767.

(27)   Barhoum, A.; Pal, K.; Rahier, H.; Uludag, H.; Kim, I. S.; Bechelany, M. Nanofibers as New-Generation Materials: From Spinning and Nano-Spinning Fabrication Techniques to Emerging Applications. *Appl. Mater. Today* **2019**, *17*, 1–35. https://doi.org/10.1016/j.apmt.2019.06.015.

(28)   Graniel, O.; Weber, M.; Balme, S.; Miele, P.; Bechelany, M. Atomic Layer Deposition for Biosensing Applications. *Biosens. Bioelectron.* **2018**, *122*, 147–159. https://doi.org/10.1016/j.bios.2018.09.038.

(29)   Weber, M.; Julbe, A.; Ayral, A.; Miele, P.; Bechelany, M. Atomic Layer Deposition for Membranes: Basics, Challenges, and Opportunities. *Chem. Mater.* **2018**, *30* (21), 7368–7390. https://doi.org/10.1021/acs.chemmater.8b02687.

(30)   Abou Chaaya, A.; Le Poitevin, M.; Cabello-Aguilar, S.; Balme, S.; Bechelany, M.; Kraszewski, S.; Picaud, F.; Cambedouzou, J.; Balanzat, E.; Janot, J. M.; et al. Enhanced Ionic Transport Mechanism by Gramicidin A Confined Inside Nanopores Tuned by Atomic Layer Deposition. *J. Phys. Chem. C* **2013**, *117* (29), 15306–15315. https://doi.org/10.1021/jp403330d.

(31)   Li, C.; Furuta, M.; Matsuda, T.; Hiramatsu, T.; Furuta, H.; Hirao, T. RF Power and Thermal Annealing Effect on the Properties of Zinc Oxide Films Prepared by Radio Frequency Magnetron Sputtering. *Res. Lett. Mater. Sci.* **2007**, *2007*, 1–5. https://doi.org/10.1155/2007/26459.

(32)   Fu, X.; Liao, Z. M.; Liu, R.; Lin, F.; Xu, J.; Zhu, R.; Zhong, W.; Liu, Y.; Guo, W.; Yu, D. Strain Loading Mode Dependent Bandgap Deformation Potential in ZnO Micro/Nanowires. *ACS Nano* **2015**, *9* (12), 11960–11967. https://doi.org/10.1021/acsnano.5b04617.

(33)   Sahoo, S.; Sharma, G. L.; Katiyar, R. S. Raman Spectroscopy to Probe Residual Stress in ZnO Nanowire. *J. Raman Spectrosc.* **2012**, *43* (1), 72–75. https://doi.org/10.1002/jrs.3004.

(34)   Reshchikov, M. A.; Kvasov, A. A.; Bishop, M. F.; McMullen, T.; Usikov, A.; Soukhoveev, V.; Dmitriev, V. A. Tunable and Abrupt Thermal Quenching of Photoluminescence in High-Resistivity Zn-Doped GaN. *Phys. Rev. B - Condens. Matter Mater. Phys.* **2011**, *84* (7), 075212. https://doi.org/10.1103/PhysRevB.84.075212.

(35) Reshchikov, M. A. Determination of Acceptor Concentration in GaN from Photoluminescence. *Appl. Phys. Lett.* **2006**, *88* (20), 202104. https://doi.org/10.1063/1.2204835.

(36) Wang, X. J.; Vlasenko, L. S.; Pearton, S. J.; Chen, W. M.; Buyanova, I. A. Oxygen and Zinc Vacancies in As-Grown ZnO Single Crystals. *J. Phys. D. Appl. Phys.* **2009**, *42* (17), 175411. https://doi.org/10.1088/0022-3727/42/17/175411.

(37) Xu, S.; Wang, Z. L. One-Dimensional ZnO Nanostructures: Solution Growth and Functional Properties. *Nano Res.* **2011**, *4* (11), 1013–1098. https://doi.org/10.1007/s12274-011-0160-7.

(38) Thomas, D. G. The Exciton Spectrum of Zinc Oxide. *J. Phys. Chem. Solids* **1960**, *15* (1–2), 86–96. https://doi.org/10.1016/0022-3697(60)90104-9.

(39) Meyer, B. K.; Alves, H.; Hofmann, D. M.; Kriegseis, W.; Forster, D.; Bertram, F.; Christen, J.; Hoffmann, A.; Straßburg, M.; Dworzak, M.; et al. Bound Exciton and Donor-Acceptor Pair Recombinations in ZnO. *Phys. Status Solidi Basic Res.* **2004**, *241* (2), 231–260. https://doi.org/10.1002/pssb.200301962.

TOC Graphic